ELSEVIER

Contents lists available at ScienceDirect

Journal of Solid State Chemistry

journal homepage: www.elsevier.com/locate/jssc



A humidity-controlled precipitation technique enabling discovery of $Rb_3(H_{1.5}PO_4)_2$



Sheel Sanghvi^a, Sossina M. Haile a,b,c,*

- ^a Department of Material Science and Engineering, Northwestern University, Evanston, IL, USA
- ^b Applied Physics, Northwestern University, Evanston, IL, USA
- ^c Department of Chemistry, Northwestern University, Evanston, IL, USA

ARTICLE INFO

Keywords: Crystal Growth Precipitation Humidity Solid Acid Cs₃H(SeO₄)₂ Cs₃(H_{1.5}PO₄)₂

ABSTRACT

The previously unknown compound $Rb_3(H_{1.5}PO_4)_2$ is successfully synthesized here using a newly developed variant of aqueous precipitation crystal growth. The approach exploits the phenomenon of boiling point elevation in concentrated solutions. Crystals of the title compound were obtained upon heating a stoichiometric solution from 110 to 150 °C under a high steam partial pressure of 0.83 atm. Single crystal X-ray diffraction studies revealed $Rb_3(H_{1.5}PO_4)_2$ crystallizes in space group C2/m and is isostructural to $Cs_3(H_{1.5}PO_4)_2$. As evidenced by thermal analysis, $Rb_3(H_{1.5}PO_4)_2$ does not undergo a phase transition to a trigonal superprotonic phase upon heating. Even under a steam partial pressure of 0.82 atm, under which dehydration is suppressed to a temperature of 263 °C, no polymorphic transition is detected. The behavior parallels that of $Cs_3(H_{1.5}PO_4)_2$ and contrasts that of several structurally and chemically similar selenate compounds. The crystal growth approach developed here may prove particularly useful for obtaining water soluble compounds which are thermodynamically or kinetically disfavored at temperatures close to ambient.

1. Introduction

Solid acids with superprotonic conductivity continue to garner interest as electrolytes in electrochemical cells for clean energy technologies, in particular fuel cells for converting hydrogen or other fuels into electricity. Within this class, CsH₂PO₄ has been pursued for technological implementation because it displays chemical stability against reaction with either hydrogen or oxygen along with the requisite high conductivity (10⁻² S/cm at 250 °C) [1,2]. All other known superprotonic solid acids bear sulfate or selenate polyanion groups, e.g., CsHSO₄, Cs₃H(SeO₄)₂, and are unstable with respect to formation of H₂S or H₂Se on exposure to H₂, a reaction that is moreover accelerated in the presence of Pt, typically utilized as a fuel cell electrocatalyst [3,4]. While the properties of CsH₂PO₄ are sufficient to warrant the development of commercial products, this electrolyte suffers from thermally induced decomposition unless high levels of humidity are provided to suppress the dehydration reaction [5-7]. The new solid acid phosphate $Cs_3(H_{1.5}PO_4)_2$ [8,9] is essentially isostructural to $M_3H(XO_4)_2$ (M = Cs, Rb, K, NH_4 ; X = S, Se) compounds that undergo a superprotonic transition from their respective room temperature monoclinic phases to a high conductivity trigonal phase, with a transition temperature between ~ 60 and 180 °C, depending on composition. Surprisingly, the phosphate does not undergo a superprotonic transition prior to decomposition, even under an atmosphere of full steam (water partial pressure, $pH_2O\sim 1$ atm) [8,9]. The discovery of $Cs_3(H_{1.5}PO_4)_2$ and its unexpected phase behavior motivates efforts to synthesize analogous compounds of the form $M_3(H_{1.5}PO_4)_2$ (M = Li, Na, K, Rb, Cs). The results reported here describe the new compound $Rb_3(H_{1.5}PO_4)_2$.

To date, no evidence of the existence of $Rb_3(H_{1.5}PO_4)_2$ has been presented. On the contrary, Gaydamaka et al. [10] have shown that solid state reaction at 55 °C between RbH_2PO_4 and Rb_2HPO_4 in equimolar concentration, corresponding to $Rb_3(H_{1.5}PO_4)_2$, produces a mixture of $Rb_5H_7(PO_4)_4$ and Rb_2HPO_4 . Attempts here to obtain $Rb_3(H_{1.5}PO_4)_2$ by precipitation at room temperature from an aqueous solution with a stoichiometric 3:2 M ratio of $Rb^+:PO_4^{3-}$, again corresponding to the stoichiometry of $Rb_3(H_{1.5}PO_4)_2$, produced crystals of $Rb_5H_7(PO_4)_4$. The failure of these efforts to yield $Rb_3(H_{1.5}PO_4)_2$ does not preclude its possible existence as a stable phase. For example, the compound $Rb_5H_3(SO_4)_4$ does not form at ambient temperatures, but is readily synthesized at temperatures above ~ 150 °C by high temperature solid state reaction [11]. Furthermore, even the most favorable thermodynamic phases may be difficult to obtain due to kinetic competition from

^{*} Corresponding author. Department of Material Science and Engineering, Northwestern University, Evanston, IL, USA. *E-mail addresses*: sheel@u.northwestern.edu (S. Sanghvi), sossina.haile@northwestern.edu (S.M. Haile).

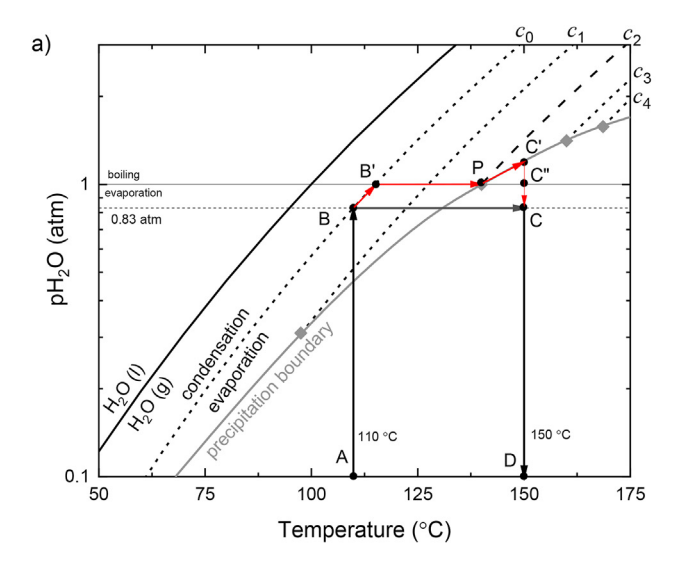
other phases. Here we report the growth of crystals of the new compound $Rb_3(H_{1.5}PO_4)_2$ realized using high-temperature, humidity-controlled precipitation. The material is isostructural to $Cs_3(H_{1.5}PO_4)_2$. Like the Cs analog, $Rb_3(H_{1.5}PO_4)_2$ does not transform upon heating to a trigonal phase prior to dehydration, although the dehydration may be preceded by a subtle polymorphic transformation.

2. Crystal growth

Growth of single crystals of solid acid compounds is readily achieved by controlled precipitation from aqueous solution. The principle is straight-forward. A solution is held at a temperature at which evaporation of $\rm H_2O$ occurs such that the concentration of solute gradually exceeds the solubility limit. Implementing this strategy at temperatures above 100 °C, at which we speculated $\rm Rb_3(H_{1.5}PO_4)_2$ is favored, appears at first glance, to be impossible in the absence of high total pressure because $\rm H_2O$ boils under such conditions. However, a high concentration of salt in the aqueous solution will shift the vapor-liquid phase boundary to high temperatures relative to pure $\rm H_2O$, a phenomenon commonly

referred to as boiling point elevation [12]. We exploited this behavior to access temperatures above 100 $^{\circ}$ C for aqueous crystal growth.

The overall growth strategy can be understood in terms of the steps indicated in Fig. 1(a), a hypothetical, but representative, phase diagram; a schematic of the apparatus is presented in Fig. 1(b). The salt is first allowed to equilibrate with steam under elevated temperature (T) and water partial pressure (pH₂O), by bringing the material from state A to state B. The solid absorbs H₂O from the gas atmosphere, undergoing deliquescence, until reaching a saturation concentration, c_0 . The concentration in the equilibrated solution corresponds to that which has its liquid-vapor equilibrium line passing through condition B, shown as the left-most dashed line. The temperature of the system is then raised, while leaving the inlet water partial pressure unchanged, bringing the environmental conditions to C, at which the apparatus is held for a prolonged period. Because the solution composition does not respond instantaneously to the temperature change, the vapor pressure of the solution rises until it reaches 1 atm, state B'. From this point onwards, evaporation proceeds quickly and the solution becomes increasing concentrated. The state of the solution moves from B' towards C", with the salt



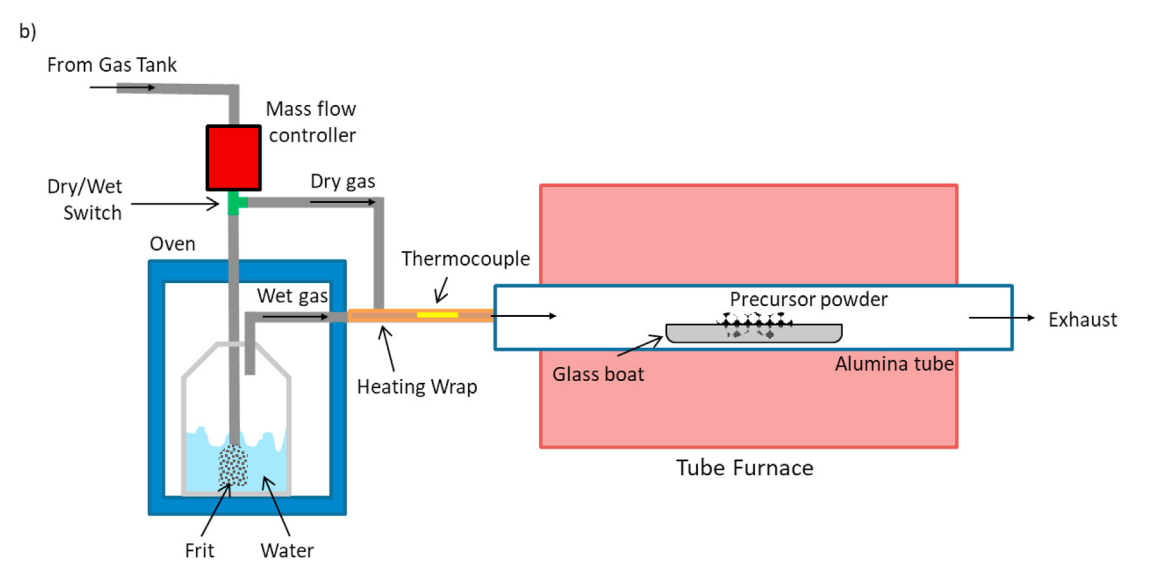


Fig. 1. Synthesis strategy for achieving crystal growth from high temperature aqueous solution: (a) Hypothetical phase diagram describing crystal growth pathway at temperatures above 100 °C; and (b) schematic of experimental apparatus. In (a) the solid black line is the liquid-vapor phase boundary of pure water, the dashed black lines are hypothetical liquid-vapor phase boundaries for salt solutions of varying concentrations, c_i , with $c_0 < c_1 < c_2 < c_3 < c_4$, and the solid grey line is the precipitation boundary mapped from the hypothetical liquidus line of the associated temperature-concentration phase diagram. The crystal growth is achieved by changing the global system state from B to C, causing the solution to follow the example trajectory indicated by the red arrows. See text for further discussion. (For interpretation of the references to colour in this figure legend, the reader is referred to the Web version of this article.)

concentrations $\{c_i\}$ having values $c_0 < c_1 < c_2 < c_3 < c_4$. At some concentration along this journey, the maximum solubility is reached, and the solution enters a regime in which the condensed phase is a solid-liquid mixture. That is, the solution concentration crosses the precipitation boundary (solid grey line), a boundary fixed by the locus of points corresponding to the temperature-dependent liquidus line of the associated temperature-concentration phase diagram. Depending on the details of the liquidus boundary, the equilibrium vapor pressure over such a condensed phase might now be expected to exceed 1 atm, following, for example, the trajectory P to C'. So long as the maximum solubility lies below the concentration c_4 that would display a hypothetical liquidvapor equilibrium boundary passing through position C, where condition C corresponding to the T and pH₂O of the external parameters during the crystal growth period, H₂O evaporation occurs under the hold conditions, and a dry, crystalline solid is ultimately produced. To avoid possible deliquescence on cooling, the pH2O is lowered (to attain condition D) before reducing the temperature.

The procedure was implemented here according to the following specific steps. First, RbH₂PO₄ was synthesized as one of the reagents. This material was obtained by methanol-induced precipitation from an aqueous solution of 1:2 M Rb₂CO₃ (Alfa Aesar, 99.9% metals basis) and H₃PO₄ (Sigma Aldrich, 85 wt%). The product was vacuum filtered and confirmed to be phase pure RbH₂PO₄ by X-ray powder diffraction (not shown). A stoichiometric mixture of this RbH2PO4 and Rb2CO3 was placed in a quartz boat and heated in a furnace to 110 °C. An inlet gas stream of water vapor with $pH_2O = 0.83$ atm, achieved by flowing O_2 through a water bubbler at 95 °C, was then supplied and the sample held at this condition for approximately 30 min. The precursors quickly underwent deliquescence to form an aqueous solution (condition B). Following the initial equilibration and while maintaining the high water vapor, the furnace temperature was raised to 150 °C at a heating rate of 2 °C/min and held for 24 h (condition C), eventually generating the crystalline product. In the final step, the supply of water vapor was turned off, and the apparatus was allowed to cool in flowing, nominally dry O2 to room temperature. The product was completely dry and formed of submillimeter transparent crystals in a bed of white powder, identified in subsequent experiments to be material of the same phase. The material was stored in a dry 150 °C oven until subsequent characterization.

3. Characterization

Single crystal X-ray diffraction (SCXRD) data were collected at -173°C (100 K) under flowing nitrogen using a Bruker APEX II diffractometer equipped with an Incoatec Microfocus Mo Kα source and HELIOS MX multilayer optics. The selected crystal was found to display nonmerohedral twinning (i.e., was an intergrowth of two crystals with random orientation with respect to one another). A multi-scan absorption correction was applied using SADABS and twinning was accounted for using TWINABS. The crystal structure was solved by direct methods using SHELXS in the OLEX2 GUI and refined with SHELXL [13-15]. Powder X-ray diffraction (PXRD) was performed at the growth temperature of 150 °C and at ambient temperature using a Rigaku Ultima IV diffractometer (Cu Kα source) fitted with a custom, high-temperature stage [9]. In both cases data were collected under ambient laboratory atmosphere (\sim 25 °C, \sim 35% relative humidity). Rietveld refinement of the structure model was performed using the program GSAS-II [16]. Parameters refined were background, scale factor, sample displacement, Lorentzian broadening, spherical harmonic preferred orientation, lattice constants, and isotropic displacements, with a single Uiso for all elements of the same type.

Simultaneous TGA and DSC of Rb₃($H_{1.5}PO_4$)₂ was performed using a Netzsch STA 449 F3 equipped with a water vapor furnace for controlling pH_2O in the range 0–1 atm. Humidification was obtained by injecting steam into Ar. Samples ~30 mg in mass were heated to 150 °C and held for 1 h under flowing dry Ar to remove surface absorbed water. Thermal profiles were then measured under both dry and humidified

environments. For measurements under dry conditions, samples were directly heated to 500 °C at 0.5 °C/min. For measurements under humidity, the desired level of humidification ($p\mathrm{H}_2\mathrm{O}=0.22,\,0.43,\,\mathrm{or}\,0.82$ atm, balance Ar) was introduced at 150 °C, and the samples were equilibrated for 1 h before further heating to 500 °C at 0.5 °C/min. The recorded data were smoothed to remove artifacts due to periodic $\mathrm{H}_2\mathrm{O}$ condensation.

4. Results and discussion

The crystals obtained from the high-temperature, high-humidity crystallization process were found to be $Rb_3(H_{1.5}PO_4)_2$. Crystal data and structure refinement information are listed in Table 1. Atomic parameters and anisotropic displacement parameters are provided in Tables 2 and 3, respectively. Rb₃(H_{1.5}PO₄)₂ adopts the C2/m space group, identical to Cs₃(H_{1.5}PO₄) [9]. Excluding proton positions, both compounds are isostructural to $Cs_3H(SeO_4)_2$ [17–19]. The X-ray powder diffraction pattern (collected at 150 $^{\circ}$ C) is fully accounted for by the structure obtained from the low temperature single crystal structure determination, Fig. 2(a). Cell parameters from the powder data refined to a = 10.668(2), b =6.1326(3), c = 7.5420(8) Å, and $\beta = 108.068(3)$ °, indicating a 2.6% cell volume contraction between 150 °C and −173 °C. Powder diffraction measurements at room temperature, Fig. 2(b), revealed a gradual transformation to an unidentified crystalline hydrate phase. Exposure to 150 °C recovered the Rb₃(H_{1.5}PO₄)₂ phase. It is this hydration behavior that required storage (or treatment) of the material at 150 °C prior to characterization.

As shown in Fig. 3, the Rb and PO_4 ions in $Rb_3(H_{1.5}PO_4)_2$ are arranged in a pseudo-hexagonal arrangement, a feature typical of $M_3H(XO_4)_2$ compounds [20]. Each of the crystallographically distinct Rb cations is surrounded by a coordination polyhedron of ten oxygen atoms, with Rb – O bond distances ranging from 2.83 to 3.45 Å, Table 4. The single, crystallographically distinct PO_4 tetrahedron is slightly distorted, Table 5, with bond distances ranging from 1.50 to 1.57 Å and angles deviating by no more than 3° from the ideal value of 109.5° .

The hydrogen atoms, H(1) and H(2), are associated with the oxygen atoms of the two longer P-O bonds, in agreement with the reported correlation between hydrogen bond lengths and P-O bonds distances of $H_2PO_{4-\ anions\ [21].\ As\ in\ Cs3}(H_{1.5}PO_4)$ [9], the phosphate groups are linked

Table 1
Crystal data and structure refinement information for Rb₃(H_{1.5}PO₄)₂.

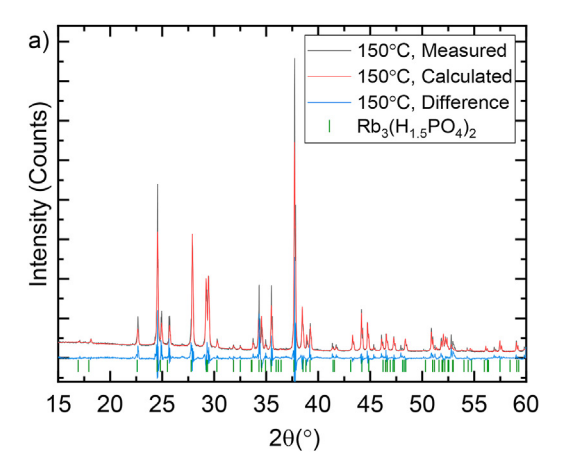
Empirical formula Rb ₃ H ₃ O ₈ P ₂ Formula weight 449.37 amu Temperature 100 K	
Temperature 100 K	
remperature 100 K	
Crystal system Monoclinic	
Space group C2/m	
Unit-cell dimensions $a = 10.611(2) \text{ Å}$	
b = 6.0390(9) Å	
c = 7.5221(11) Å	
$lpha=90^\circ$	
$eta=108.534(4)~^\circ$	
$\gamma=90^\circ$	
Volume 456.99(12) Å ³	
Z 2	
Density (calculated) 3.266 g/cm ³	
Absorption coefficient 16.360 mm ⁻¹	
F(000) 416.0	
Instrument Bruker APEX II	
Radiation Mo K α ($\lambda = 0.71073$)	
2Θ range for data collection 5.712–74.248°	
$-17 \leq h \leq 16, 0 \leq k \leq 10, 0 \leq l \leq 12$ Index ranges	
Reflections collected 1259	
$\label{eq:localization} Independent \ reflections \qquad \qquad 1259 \ [R_{int} = 0.0779, \ R_{sigma} = 0.0439]$	
Data/restraints/parameters 1259/0/42	
Goodness-of-fit on F [2] 1.041	
Final R indexes [I $\geq 2\sigma$ (I)] $R_1 = 0.0371, wR_2 = 0.0828$	
Final R indexes [all data] $R_1 = 0.0513, wR_2 = 0.0888$	
Largest diff. peak/hole/e Å ⁻³ 2.12/-1.69	

Table 2 Atomic coordinates, site, occupancy, and equivalent isotropic displacement (U_{eq}) parameters for $Rb_3(H_{1.5}PO_4)_2$ at -173 °C. (C2/m a =10.611(2) Å, b =6.0390(9) Å, c =7.5221(11) Å, $\beta=108.534(4)$ °) U_{eq} is defined as one-third of the trace of the orthogonalised U_{ij} tensor.

Atom	Site	Occupancy	x	у	z	U_{eq} (Å ²)
Rb(1)	2a	1	0	0.5	0.5	0.01034(11)
Rb(2)	4i	1	0.73815(4)	0	0.14084(5)	0.01062(10)
P	4i	1	0.09974(11)	0	0.26466(14)	0.0096(2)
O(1)	8j	1	0.0156(2)	0.2100(3)	0.1741(3)	0.0110(3)
O(2)	4i	1	0.1096(3)	0	0.4749(4)	0.0139(5)
O(3)	4i	1	0.2332(3)	0	0.235(4)	0.0118(5)
H(1)	4h	1	0	0.19(2)	0	0.14(5)
H(2)	2b	1	0	0	0.5	0.09(5)

Table 3 Anisotropic displacement parameters for $Rb_3(H_{1.5}PO_4)_2$ at $-173~^{\circ}C$.

Atom	U_{11} (\mathring{A}^2)	$\mathrm{U}_{22}(\mathring{\mathrm{A}}^2)$	$\mathrm{U}_{33}\ (\mathrm{\mathring{A}}^2)$	$\mathrm{U}_{23}(\mathring{\mathrm{A}}^2)$	U_{13} (\mathring{A}^2)	U_{12} (Å ²)
Rb(1)	0.0120(3)	0.0083(2)	0.0105(2)	0	0.0034(2)	0
Rb(2)	0.0119(2)	0.00936(14)	0.0119(2)	0	0.00567(13)	0
P	0.0093(5)	0.0109(4)	0.0084(4)	0	0.0026(3)	0
O(1)	0.0125(10)	0.0096(7)	0.0112(8)	-0.0014(6)	0.0040(7)	0.0027(6)
O(2)	0.0127(15)	0.0207(13)	0.0085(11)	0	0.0033(10)	0
O(3)	0.0096(14)	0.0140(11)	0.0133(12)	0	0.0058(10)	0



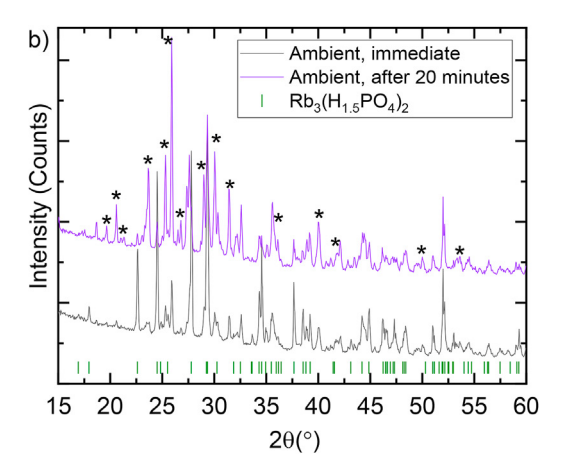


Fig. 2. PXRD patterns collected from $Rb_3(H_{1.5}PO_4)_2$: (a) at 150 °C and (b) under ambient conditions of ~25 °C and ~35% relative humidity. In (a) the pattern is fully described by the structure determined for $Rb_3(H_{1.5}PO_4)_2$ at -173 °C, as indicated by the agreement between the measured (black) and calculated (red) patterns. In (b) evolution of the patterns is evident, with the peaks of a secondary phase (*), presumed to be a hydrate, growing after 20 min of exposure to ambient conditions. (For interpretation of the references to colour in this figure legend, the reader is referred to the Web version of this article.)

by hydrogen bonds to form changes that extend along [001]. The chain linkages alternate between a single P-O(2)-H(2)-O(2)-P bond and a pair of P-O(1)-H(1)-O(1)-P bonds. Thus, there are three such bonds per phosphate group and the O(1) and O(2) atoms simultaneously serve as donor and acceptor in their respective hydrogen bonds. Refinement of the proton positions suggested these atoms both reside at single-minimum, high symmetry positions equidistant from the oxygen atoms, Table 6. While the O(2) ... O(2) distance of 2.472(7) Å is consistent with such a configuration, the O(1) ... O(1) distance of 2.533(5) Å is atypically long for a single-minimum hydrogen bond [22, 23], particularly given the low temperature of the measurement. The result also contrasts what was found in Cs₃(H_{1.5}PO₄)₂, in which a double-minimum hydrogen bond was resolved at this location [9]. The structure solution here, which also yields unusually large displacement parameters for the protons, may be influenced by the twinned nature of the crystal employed in the measurement, and also points to the difficulties that can be encountered when trying to use x-ray diffraction to obtain proton positions with high accuracy in compounds containing heavy elements.

The TGA profiles of Rb₃(H_{1.5}PO₄)₂ under various humidities are

presented in Fig. 4(a). Under dry conditions, the onset of $Rb_3(H_{1.5}PO_4)_2$ dehydration, indicated by mass loss, begins at $\sim 215\,^{\circ}C$ and reaches completion at $\sim 375\,^{\circ}C$. If dehydration proceeds in a manner similar to that of $Cs_3(H_{1.5}PO_4)_2$, then the expected dehydration reaction is [8]:

$$2 \text{ Rb}_3(\text{H}_{1.5}\text{PO}_4)_2 \rightarrow 2 \text{RbPO}_3 + \text{Rb}_4\text{P}_2\text{O}_7 + 3\text{H}_2\text{O}$$

The theoretical weight loss of 6.0 wt% matches the measured weight loss of 5.9 wt%. As humidity is increased, the onset of dehydration (T_d) is shifted to 255, 260, and 263 °C for pH_2O levels of 0.22, 0.43, and 0.82 atm, respectively. Moreover, the dehydration under these conditions occurs via two clear steps, in contrast to the gradual mass loss evident under dry conditions, with the first of these steps further resolving into a two-step process at high pH_2O . The DSC profiles recorded under active humidification, Fig. 4(b), show strong thermal anomalies corresponding to the temperatures of the dehydration events, with a similar upwards shift in temperature with increasing humidification level and resolution of the dehydration phenomenon into multiple steps. A close examination of the DSC profiles just prior to the first dehydration event reveals a very small thermal anomaly with an onset temperature of ~251 °C. Because of the weak intensity of this peak, complete characterization was not

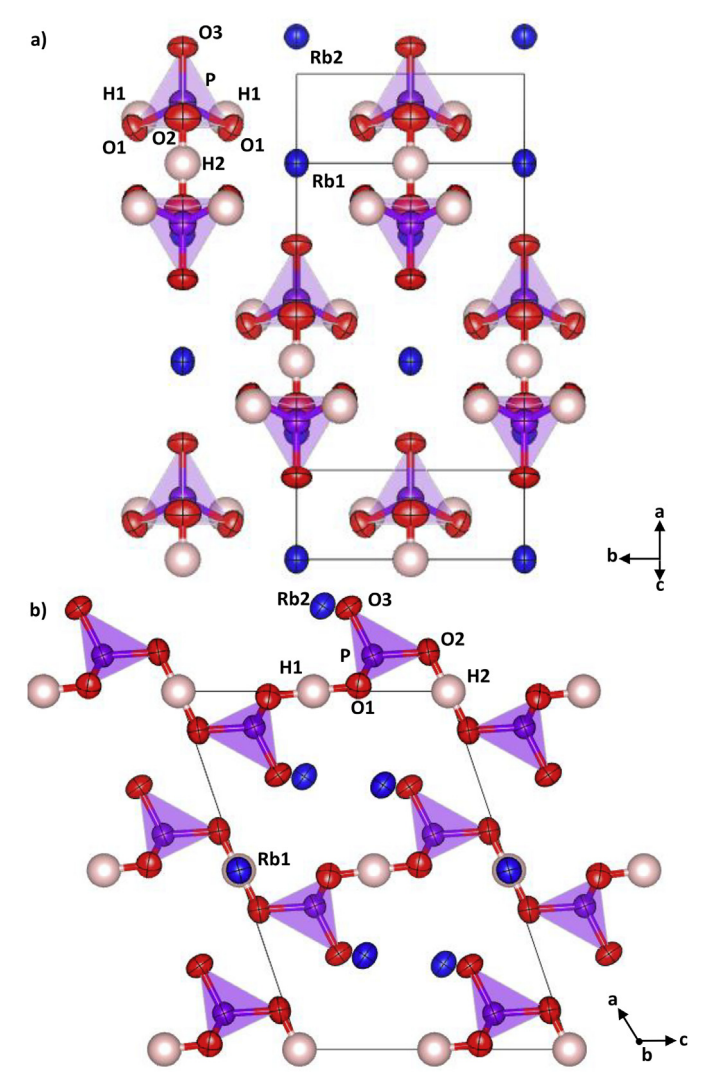


Fig. 3. The crystal structure of $Rb_3(H_{1.5}PO_4)_2$ shown in projection: (a) along the c^* direction, and (b) along the b direction. In (b) the labeled H1 atom occurs at elevation y = -0.19; another O1–H1–O1 bond, with the proton at elevation y = 0.19 (and identical x and z coordinates), also links the same pair of phosphate groups. Such linkages, along with the O2–H2–O2 bonds, create a hydrogen bonded chain of alternating single and double hydrogen bonds that extends along c.

Table 4 Bond distances in the Rb–O coordination polyhedron of Rb₃(H_{1.5}PO₄)₂ at -173 °C. Multiplicity of the bond is indicated by \times #.

Atom	Atom	Distance (Å)
Rb(1)	O(1)	3.060(2) × 4
Rb(1)	O(2)	3.2629(13) × 4
Rb(1)	O(3)	$2.898(3) \times 2$
Rb(2)	O(1)	$3.013(2) \times 2$, $3.142(2) \times 2$, $3.446(2) \times 2$
Rb(2)	O(2)	$2.828(3) \times 1$
Rb(2)	O(3)	$2.938(3) \times 1, 3.1058(8) \times 2$

possible. However, in contrast to the dehydration processes, it was generally found (from a study of multiple samples, not shown) to be invariant with $p\rm H_2O$, and thus not a result of loss of $\rm H_2O$ from the structure. Given the small thermal signature, it is unlikely that this thermal event corresponds to a transformation to a superprotonic trigonal phase, as is known in several $\rm M_3H(SeO_4)_2$ analogs [24]. In $\rm Cs_3(\rm H_{1.5}PO_4)_2$, heating induces a partial exsolution of a small amount of a $\rm CsH_2PO_4$ -like phase, and it is possible a similar phenomenon occurs in

Table 5 Bond distances and angles in the phosphate tetrahedron of Rb $_3(H_{1.5}PO_4)_2$ at $-173\,^{\circ}C$

Atom	Atom	Distance (Å)	Atom	Atom	Atom	Angle (°)
P	O(1)	1.575(2)	O(1)	P	O(1)	107.2(2)
P	O(2)	1.551(3)	O(1)	P	O(2)	106.63(10)
P	O(3)	1.502(3)	O(1)	P	O(3)	111.54(10)
			O(2)	P	O(3)	112.9(2)

Table 6 Hydrogen bond environment of $Rb_3(H_{1.5}PO_4)_2$ at -173 °C.

Atoms			Distance (Å)		Angle (°)	
Donor(D) Hydrogen(H) Acceptor		Acceptor(A)	O _{D/A} – H	O _{D/A} ··· O _{D/A}	O – H – O	
O(1) O(2)	H(1) H(2)	O(1) O(2)	1.272(13) 1.236(4)	2.533(5) 2.472(7)	169(11) 180	

Rb₃(H_{1.5}PO₄)₂. As discussed in the context of Cs₃(H_{1.5}PO₄)₂ [8,9], the absence of a superprotonic transition in M₃(H_{1.5}PO₄)₂ compounds and Rb₃H(SO₄)₂ [5,25] may be connected to the relatively short O(2) ... O(2) bond and, in the case of the phosphates, the overall high number of hydrogen bonds that stabilize the monoclinic structure.

5. Conclusions

In this work we demonstrate a humidity-controlled precipitation process that enables the discovery of Rb₃(H_{1.5}PO₄)₂. At ambient temperature and atmosphere (~25 °C, ~35% relative humidity) the compound transforms to an unidentified hydrate phase, presumably contributing to the difficulties encountered in prior attempts to crystallize $Rb_3(H_{1.5}PO_4)_2$ at temperatures below 150 °C. While the synthesis approach can be considered a variant of conventional aqueous precipitation, it differs in that it exploits the chemical characteristics of highly concentrated solutions. In particular, the liquid-vapor phase boundary of such solutions is naturally, and potentially very strongly, shifted towards high temperature relative to pure water. When combined with a high level of humidity in the flowing gas stream, the precipitation/crystal growth step can be carried out at temperatures much higher than 100 °C, providing access to water-soluble phases that may be inaccessible at lower temperatures. Furthermore, though not demonstrated here, the approach can, in principle, be expanded such that the oxygen or hydrogen partial pressure in the humidified gas stream is also actively regulated, providing additional control over the synthesis outcome. Hydrothermal synthesis provides access to similarly high temperatures and even higher pressures, however, it is restricted to the growth of sparingly soluble materials and, due to the fully sealed environment, is incompatible with independent control of gas-phase chemical potential [26]. The synthesis approach demonstrated here offers the additional advantage of a relatively simple experimental set-up, requiring little more than a high temperature oven and a heated water bubbler.

The new compound Rb₃(H_{1.5}PO₄)₂ discovered through this synthetic process crystallizes in space group C2/m and is isostructural to Cs₃(H_{1.5}PO₄)₂. In contrast to structurally and chemically similar compounds like Cs₃H(SeO₄)₂ and Rb₃H(SeO₄)₂, Rb₃(H_{1.5}PO₄)₂ does not undergo a phase transition to a trigonal superprotonic phase upon heating, even under a steam partial pressure of 0.82 atm, under which dehydration is suppressed to a temperature of 263 °C. The absence of a superprotonic phase parallels the behavior of Cs₃(H_{1.5}PO₄)₂. A small thermal anomaly is detected just prior to dehydration and may reflect the partial exsolution of a minor phase, as has been observed in Cs₃(H_{1.5}PO₄)₂.

CRediT authorship contribution statement

Sheel Sanghvi: Conceptualization, Investigation, Writing - original

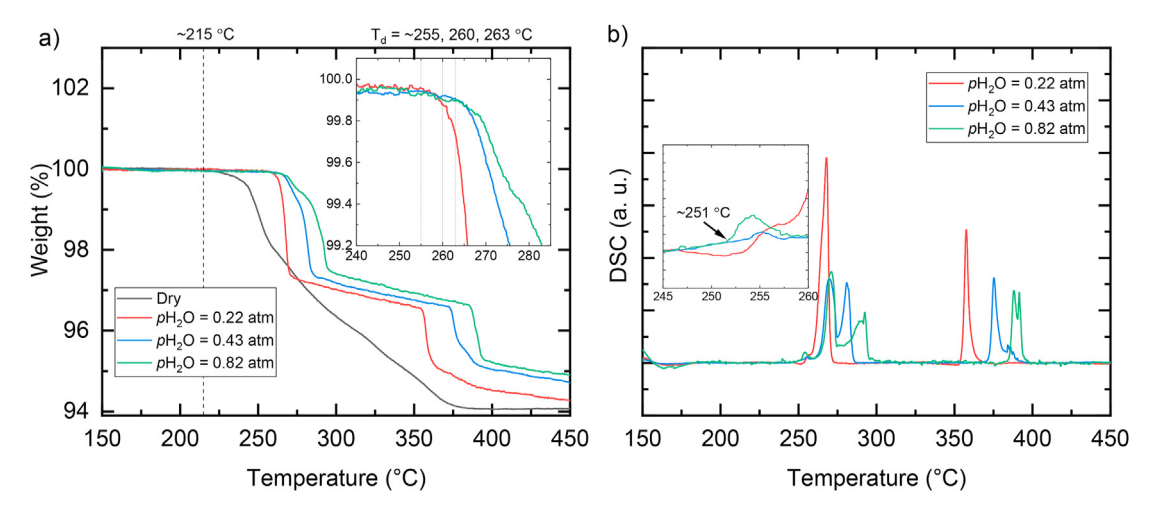


Fig. 4. Thermal analysis of $Rb_3(H_{1.5}PO_4)_2$ under the atmospheres indicated: (a) TGA, and (b) DSC profiles. Inset in (a) highlights the mass loss behavior between 240 and 285 °C, whereas that in (b) highlights the thermal behavior between 245 and 260 °C.

draft, Writing - review & editing. **Sossina M. Haile:** Supervision, Writing - review & editing, Funding acquisition.

Declaration of competing interest

The authors declare that they have no known competing financial interests or personal relationships that could have appeared to influence the work reported in this paper.

Acknowledgements

Financial support has been provided by National Science Foundation (DMR 1807234). SCXRD experiments made use of the Integrated Molecular Structure Education and Research Center (IMSERC) at Northwestern University, which has received support from SHyNE, the State of Illinois and International Institute for Nanotechnology (IIN). The authors thank Charlotte Stern for single crystal data collection.

References

- D.A. Boysen, S.M. Haile, H. Liu, R.A. Secco, High-temperature behavior of CsH2PO4 under both ambient and high pressure conditions, Chem. Mater. 15 (3) (2003) 277, 726
- [2] S.M. Haile, C.R.I. Chisholm, K. Sasaki, D.A. Boysen, T. Uda, Solid acid proton conductors: from laboratory curiosities to fuel cell electrolytes, Faraday Discuss 134 (2007) 17–39.
- [3] R.B. Merle, C.R.I. Chisholm, D.A. Boysen, S.M. Haile, Instability of sulfate and selenate solid acids in fuel cell environments, Energy Fuels 17 (1) (2003) 210–215.

[4] T. Uda, D.A. Boysen, S.M. Haile, Thermodynamic, thermomechanical, and

- electrochemical evaluation of CsHSO4, Solid State Ionics 176 (1) (2005) 127-133.
- [5] A. Ikeda, S.M. Haile, The thermodynamics and kinetics of the dehydration of CsH2PO4 studied in the presence of SiO2, Solid State Ionics 213 (2012) 63–71.
- [6] Y.K. Taninouchi, T. Uda, Y. Awakura, A. Ikeda, S.M. Haile, Dehydration behavior of the superprotonic conductor CsH2PO4 at moderate temperatures: 230 to 260 degrees C, J. Mater. Chem. 17 (30) (2007) 3182–3189.
- [7] D.A. Boysen, T. Uda, C.R.I. Chisholm, S.M. Haile, High-performance solid acid fuel cells through humidity stabilization, Science 303 (5654) (2004) 68.
- [8] V. Ponomareva, I. Bagryantseva, B. Zakharov, N. Bulina, G. Lavrova, E. Boldyreva, Crystal structure and proton conductivity of a new Cs₃(H₂PO₄)(HPO₄).2H₂O phase in the caesium di- and monohydrogen orthophosphate system, Acta Crystallogr. C 73 (10) (2017) 773–779.

- [9] S. Sanghvi, S.M. Haile, Crystal structure, conductivity, and phase stability of Cs3(H1.5PO4)2 under controlled humidity, Solid State Ionics 349 (2020) 115291.
- [10] A.A. Gaydamaka, V.G. Ponomareva, I.N. Bagryantseva, Phase composition, thermal and transport properties of the system based on the mono- and dihydrogen phosphates of rubidium, Solid State Ionics 329 (2019) 124–130.
- [11] C. Panithipongwut, S.M. Haile, High-temperature phase behavior in the Rb3H(SO4)(2)-RbHSO4 pseudo-binary system and the new compound Rb5H3(SO4)(4), Solid State Ionics 213 (2012) 53–57.
- [12] K.A.B.S. Dill, Molecular Driving Forces: Statistical Thermodynamics in Biology, Chemistry, Physics, and Nanoscience. Garland Science, vol. 2, Taylor & Francis Group, 2010.
- [13] O.V. Dolomanov, L.J. Bourhis, R.J. Gildea, J.A.K. Howard, H. Puschmann, OLEX2: a complete structure solution, refinement and analysis program, J. Appl. Crystallogr. 42 (2) (2009) 339–341.
- [14] G. Sheldrick, Crystal structure refinement with SHELXL, Acta Crystallogr. C 71 (1) (2015) 3–8.
- [15] G. Sheldrick, SADABS, Version 2.10, University of Göttingen, Germany, 2003.
- [16] B.H. Toby, R.B. Von Dreele, GSAS-II: the genesis of a modern open-source all purpose crystallography software package, J. Appl. Crystallogr. 46 (2) (2013) 544–549.
- [17] R. Sonntag, R. Melzer, T. Wessels, P.G. Radaelli, Cs3H(SeO4)2 at 300K by high-resolution neutron powder diffraction, Acta Crystallogr. C 53 (11) (1997) 1529–1531.
- [18] A.I. Baranov, B.V. Merinov, A.B. Tregubchenko, L.A. Shuvalov, N.M. Shchagina, Phase transitions, structure, protonic conductivity and dielectric properties of Cs3H(SeO4)2 and Cs3(H, D)(SeO4)2, Ferroelectrics 81 (1) (1988) 187–191.
- [19] B. Merinov, N. Bolotina, A. Baranov, L. Shuvalov, Crystal structure of Cs3H(SeO4)2 (T= 295 K) and its changes in phase transformations, Kristallografiya 33 (6) (1988) 1387–1392.
- [20] D. Yi, S. Sanghvi, C.P. Kowalski, S.M. Haile, Phase behavior and superionic transport characteristics of (MxRb1-x)3H(SeO4)2 (M = K or Cs) solid solutions, Chem. Mater. 31 (23) (2019) 9807–9818.
- [21] M. Ichikawa, Dependence of the distortion of the tetrahedra in acid phosphate groups H_nPO₄ (n = 1-3) on hydrogen-bond length, Acta Crystallogr. Sect. B-Struct. Commun. 43 (1987) 23–28.
- [22] M. Ichikawa, O-H vs. O...O distance correlation, geometric isotope effect in OHO bonds, and its application to symmetric bonds, Acta Crystallogr. Sect. B Struct. Sci. 34 (JUL) (1978) 2074–2080.
- [23] I.-H. Oh, Y.J. Sohn, M. Meven, G. Heger, Symmetrical hydrogen bond in SO4-H-SO4 dimer in K3H(SO4)2 by neutron diffraction, J. Phys. Soc. Jpn. 88 (12) (2019), 124601.
- [24] A. Baranov, Crystals with disordered hydrogen-bond networks and superprotonic conductivity, Review. Crystallography Reports 48 (6) (2003) 1012–1037.
- [25] L.A. Cowan, R.M. Morcos, N. Hatada, A. Navrotsky, S.M. Haile, High temperature properties of Rb3H(SO4)2 at ambient pressure: absence of a polymorphic, superprotonic transition. Solid State Ionics 179 (9) (2008) 305–313.
- [26] A. Rabenau, The role of hydrothermal synthesis in preparative chemistry, Angew Chem. Int. Ed. Engl. 24 (12) (1985) 1026–1040.